**One Pot Hydrothermal Synthesis of $Tb^{(III)}_{13}(GeO_4)_6O_7(OH)$ and $K_2Tb^{(IV)}Ge_2O_7$: Preparation of a Stable $Tb^{4+}$ Complex**

Kyle Fulle, Liurukara. D. Sanjeewa, Colin D. McMillen, Yimei Wen, Apeksha C. Rajamanthrilage, Jeffrey N. Anker, George Chumanov, Joseph W. Kolis*

*Department of Chemistry and Center for Optical Materials Science and Engineering Technologies (COMSET), Clemson University, Clemson, South Carolina 29634-0973, USA*

## Supporting Information

Additional experimental details.

Table S1: Crystallographic data for $Tb_{13}(GeO_4)_6O_7(OH)$ and $K_2TbGe_2O_7$.

Table S2. Selected interatomic distances (Å) and angles (°) for $Tb_{13}(GeO_4)_6O_7(OH)$ and $K_2TbGe_2O_7$.

Figure S1. PXRD of $Tb_{13}(GeO_4)_6O_7(OH)$.

Figure S2. PXRD of $K_2TbGe_2O_7$.

Figure S3: Elemental analysis of $Tb_{13}(GeO_4)_6O_7(OH)$.

Figure S4: Elemental analysis of $K_2TbGe_2O_7$.

Figure S5. FTIR of $Tb_{13}(GeO_4)_6O_7(OH)$ (black) and $K_2TbGe_2O_7$ (blue) from 3700-3100 $cm^{-1}$.

Figure S6. FTIR of $Tb_{13}(GeO_4)_6O_7(OH)$ (black) and $K_2TbGe_2O_7$ (blue) from 1200-400 $cm^{-1}$

Figure S7. Raman scattering from $Tb_{13}(GeO_4)_6O_7(OH)$ and $K_2TbGe_2O_7$ from 3000-3750 $cm^{-1}$.

Figure S8. Raman scattering from $Tb_{13}(GeO_4)_6O_7(OH)$ from 300-1400 $cm^{-1}$.

Figure S9. Raman scattering from $K_2TbGe_2O_7$ from 300-1400 $cm^{-1}$.

Figure S10. Photoluminescence of $Tb_{13}(GeO_4)_6O_7(OH)$.

Figure S11. Decorated Tb(2)/Tb(3) cluster with isolated $GeO_4$ units from **I**.

Synthetic details:

Single crystals of $Tb_{13}(GeO_4)_6O_7(OH)$ and $K_2TbGe_2O_7$ were grown isothermally at 700°C for 7 days using 20 *M* KOH mineralizer. The feedstock consisted of $Tb_4O_7$ (129 mg, 0.172 mmol; HEFA Rare-Earth 99.99%) and $GeO_2$ (71 mg, 0.687 mmol; Alfa Aesar 99.9%) in a 1:4 molar ratio, respectively. These components and 0.4 mL of the KOH mineralizer were loaded into a 99.9% fine silver ampule (2.5" long) that was weld sealed. The ampule was placed in a Tuttle cold seal autoclave and counter-pressured with deionized water. Two independent band heaters were strapped to the outside of the autoclave to maintain the isothermal 700°C system, and autogenously generating 200 MPa pressure. After the reaction period the autoclave was cooled to room temperature over a period of 12 hours.

Single crystal X-ray diffraction:

Single crystal structure characterization was conducted using a Bruker D8 Venture single crystal diffractometer with an Incoatec Mo Kα microfocus source and Photon 100 CMOS detector. Data were collected at room temperature using phi and omega scans, and subsequently processed and scaled using the Apex3 software suite (SAINT and SADABS). Space group determinations were unambiguously made based on the systematic absences. The structures were solved by direct methods and refined to convergence by full-matrix least squares on $F^2$ using the SHELXTL software suite.[a] All atoms were refined anisotropically. The powder X-ray diffraction data were collected using a Rigaku Ultima IV diffractometer equipped with Cu Kα radiation (λ = 1.5406 Å). Data were collected in the range of 5-65° in 2θ with a scan speed of 0.25 degree per minute with a step size of 0.02°.

[a] Sheldrick, G. M. A short history of SHELX. *Acta Crystallogr. Sect. A* **2008**, *A64*, 112−122.

Fluorescence and white light imaging:

Crystals were mounted to a slide and imaged using a Nikon AZ100 multi-zoom microscope system (Nikon Instruments, Melville, NY) equipped with a Nikon DS-Q1Mc monochrome camera (fluorescent images) or a Leica M125 Stereoscope (Leica Microsystems, Buffalo Grove, IL) equipped with a Leica DFC290 HD color camera (darkfield images). Fluorescent images were collected using a Plan Fluor 5X objective and a Nikon UV-2A filter cube (excitation = 330 to 380 nm, emission = 420+ nm). Camera exposure time was set to 30 milliseconds, and an image was collected for each crystal using the exact same exposure time and imaging parameters using Nikon NIS Elements AR Version 3.2. Darkfield images were collected using a Plan Apo 1X objective with zoom, an LED ring light, and LED gooseneck lights. Optimum lighting conditions were determined for each sample, and a series of images were collected throughout the Z-plane using Leica LAS V4.3 software. Images were exported to Helicon Focus (HeliconSoft, Kharviv, Ukraine) for z-stacking, and a 3D composite image is presented.

Photoluminescence Spectroscopy:

SYLGARD ® 184 Silicone Elastomer base (0.20g) was thoroughly mixed with SYLGARD ® 184 Silicone Elastomer curing agent (0.02 g) in a glass vial for 5 minutes. The $Tb_{13}(GeO_4)_6O_7(OH)$ powder sample (0.04 g) was incorporated in to the mixture and air bubbles were removed by placing the sample in a vacuum chamber. The mixture was then put on a cover slip to make a layer of the powdered sample incorporated PDMS film. After that, it was cured in an oven at 100°C for 15 minutes. The prepared sample was placed inside a cuvette at a 45-degree angle to the incident beam and fluorescence excitation and emission were measured. A QuantaMaster 800 High Speed Spectrofluorometer (PTI) equipped with an 814 (PTI) photomultiplier detection system was used to carry out the P.L. measurements.

Table S1. Crystallographic data for $Tb_{13}(GeO_4)_6O_7(OH)$ (**I**) and $K_2TbGe_2O_7$ (**II**).

| | **$Tb_{13}(GeO_4)_6O_7(OH)$ (I)** | **$K_2TbGe_2O_7$ (II)** |
|---|---|---|
| FW | 3014.51 | 494.30 |
| crystal system | trigonal | monoclinic |
| crystal dimension, mm | 0.05 x 0.05 x 0.04 | 0.06 x 0.05 x 0.04 |
| space group, Z | *R*-3, 3 | *C*2/*c*, 4 |
| T, °C | 25 | 25 |
| a, Å | 15.8667(6) | 10.2720(4) |
| b, Å | 15.8667(6) | 5.7273(2) |
| c, Å | 9.5266(4) | 13.3584(6) |
| β, ° | --- | 105.6890(10) |
| V, Å$^3$ | 2077.02(18) | 756.61(5) |
| dcalc, g cm$^{-3}$ | 7.230 | 4.339 |
| 2θ range, ° | 2.26-25.99 | 3.17-28.30 |
| Tmin/Tmax | 0.6483/1.0000 | 0.7382/1.0000 |
| Reflns coll./unique/obs. | 5974/908/814 | 8694/946/915 |
| μ (Mo Kα), mm$^{-1}$ | 39.218 | 18.233 |
| data/restraints/param. | 908/1/79 | 946/0/58 |
| R1, wR2 (obs. data [I> 2σ(I)]) | 0.0267, 0.0598 | 0.0148, 0.0367 |
| R1, wR2 (all data) | 0.0323, 0.0621 | 0.0158/0.0370 |
| S | 1.069 | 1.183 |

Table S2. Selected interatomic distances (Å) and angles (°) for $Tb_{13}(GeO_4)_6O_7(OH)$ and $K_2TbGe_2O_7$.

| **$Tb_{13}(GeO_4)_6O_7(OH)$ (I)** | | **$K_2TbGe_2O_7$ (II)** | |
|---|---|---|---|
| **$Tb(1)O_7$** | | **$Tb(1)O_6$** | |
| Tb(1)−O(1) | 2.551(7) | Tb(1)−O(1) x2 | 2.2505(17) |
| Tb(1)−O(2) | 2.345(7) | Tb(1)−O(3) x2 | 2.2691(18) |
| Tb(1)−O(3) | 2.211(7) | Tb(1)−O(4) x2 | 2.3745(17) |
| Tb(1)−O(4) | 2.685(7) | **$K(1)O_9$** | |
| Tb(1)−O(5) | 2.304(7) | K(1)−O(1) | 2.691(2) |
| Tb(1)−O(5) | 2.328(7) | K(1)−O(1) | 2.8499(19) |
| Tb(1)−O(6) | 2.3205(5) | K(1)−O(1) | 3.357(2) |
| **$Tb(2)O_7$** | | K(1)−O(2) | 2.7897(19) |
| Tb(2)−O(1) | 2.304(7) | K(1)−O(3) | 2.9157(19) |
| Tb(2)−O(1) | 2.468(7) | K(1)−O(3) | 2.9617(19) |
| Tb(2)−O(2) | 2.369(7) | K(1)−O(3) | 3.1360(19) |
| Tb(2)−O(3) | 2.211(7) | K(1)−O(4) | 3.102(2) |
| Tb(2)−O(3) | 2.254(7) | K(1)−O(4) | 3.2287(19) |
| Tb(2)−O(4) | 2.336(7) | **$Ge(1)O_4$** | |
| Tb(2)−O(4) | 2.638(8) | Ge(1)−O(1) | 1.7324(16) |
| **$Tb(3)O_6$** | | Ge(1)−O(2) | 1.7901(13) |
| Tb(3)−O(3) x6 | 2.339(7) | Ge(1)−O(3) | 1.7182(17) |
| **$Ge(1)O_4$** | | Ge(1)−O(4) | 1.7719(18) |
| Ge(1)−O(1) | 1.765(7) | | |
| Ge(1)−O(2) | 1.733(7) | Ge(1)−O(2)−Ge(1) | 121.56(14) |
| Ge(1)−O(4) | 1.762(7) | | |
| Ge(1)−O(5) | 1.746(7) | | |
| | | | |
| Tb(2)−O(3)−Tb(3) | 103.7(3) | | |
| Tb(2)−O(3)−Tb(3) | 102.3(3) | | |
| Tb(1)−O(5)−Tb(1) | 122.9(3) | | |

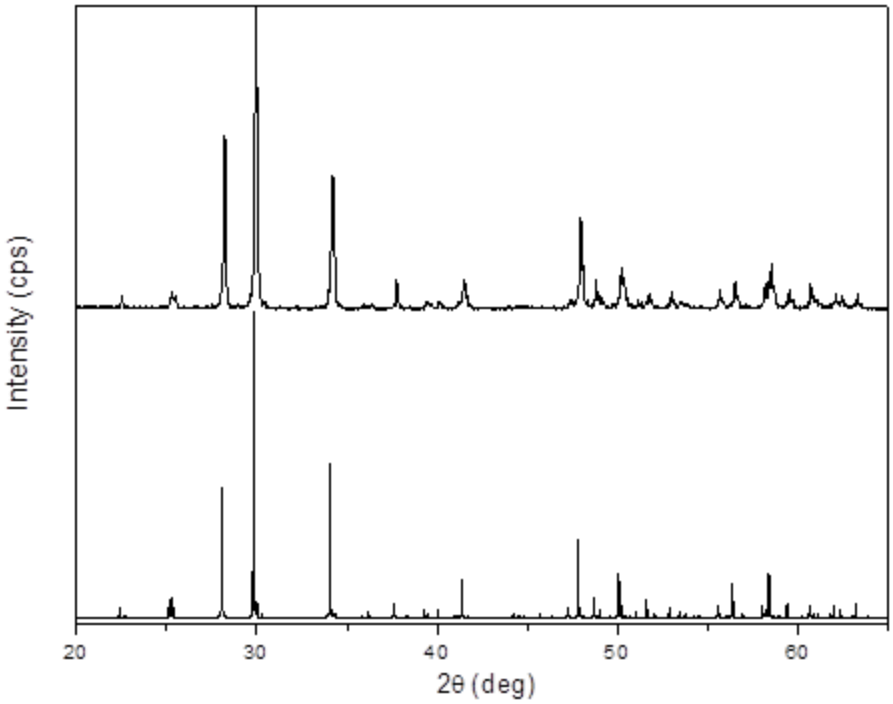


Figure S1. PXRD of $Tb_{13}(GeO_4)_6O_7(OH)$. (Top) Powder diffraction pattern of as-grown $Tb_{13}(GeO_4)_6O_7(OH)$. (Bottom) Simulated powder diffraction pattern of $Tb_{13}(GeO_4)_6O_7(OH)$ in space group *R-3*. Hydrothermally grown powder analysis was performed via the bulk material.

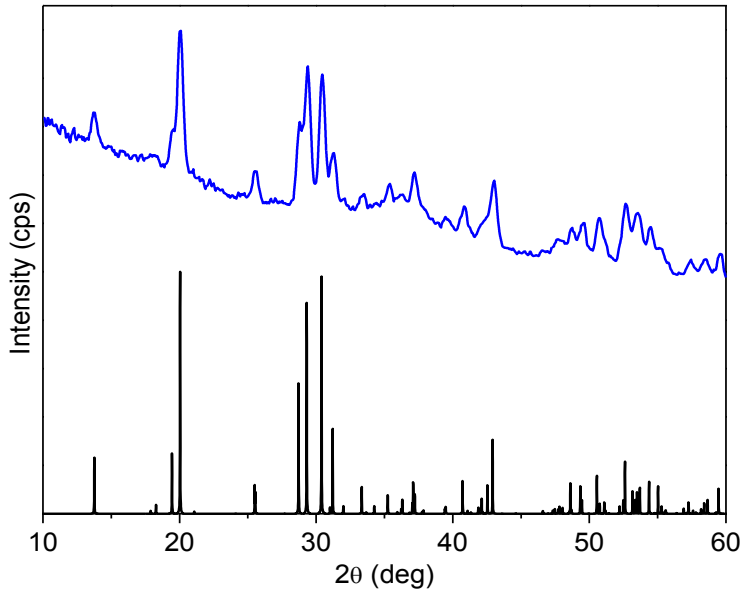


Figure S2. PXRD of $K_2TbGe_2O_7$: (Top) Powder diffraction pattern of as-grown $K_2TbGe_2O_7$. (Bottom) Simulated powder diffraction pattern of $K_2TbGe_2O_7$ in space group *C2/c*. Due to the low reaction yield, several single crystals of $K_2TbGe_2O_7$ were ground and data collected via an optimized algorithm for powder analysis using a Bruker D8 Venture single crystal diffractometer.

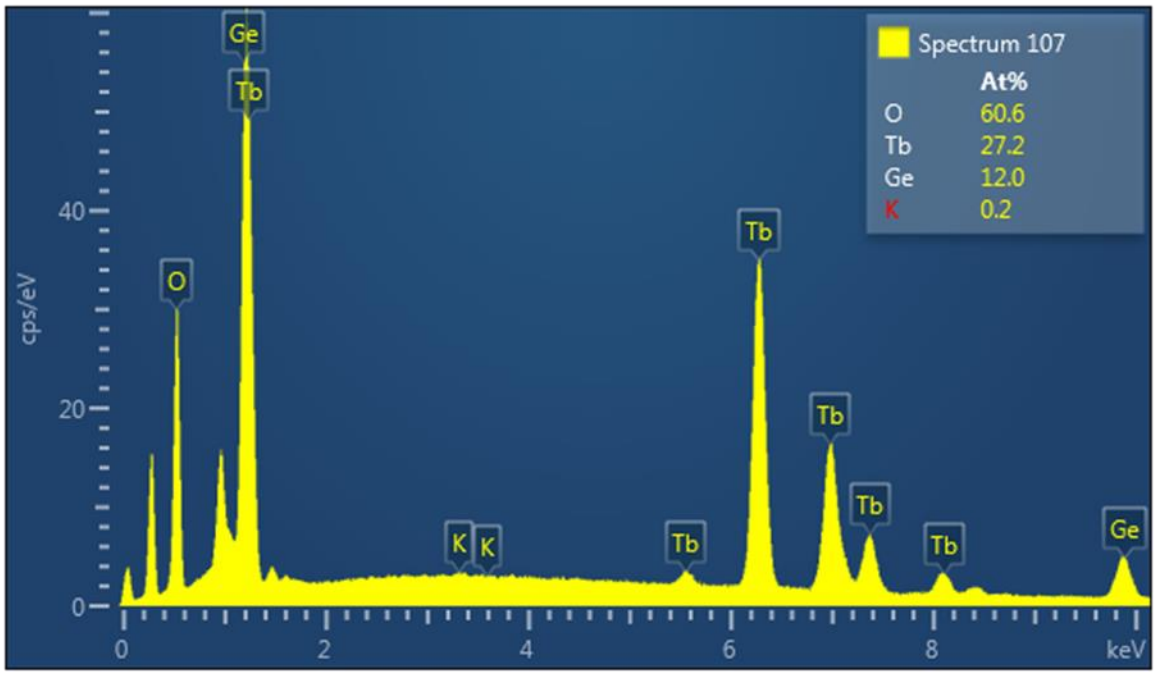


Figure S3. EDX analysis of $Tb_{13}(GeO_4)_6O_7(OH)$.

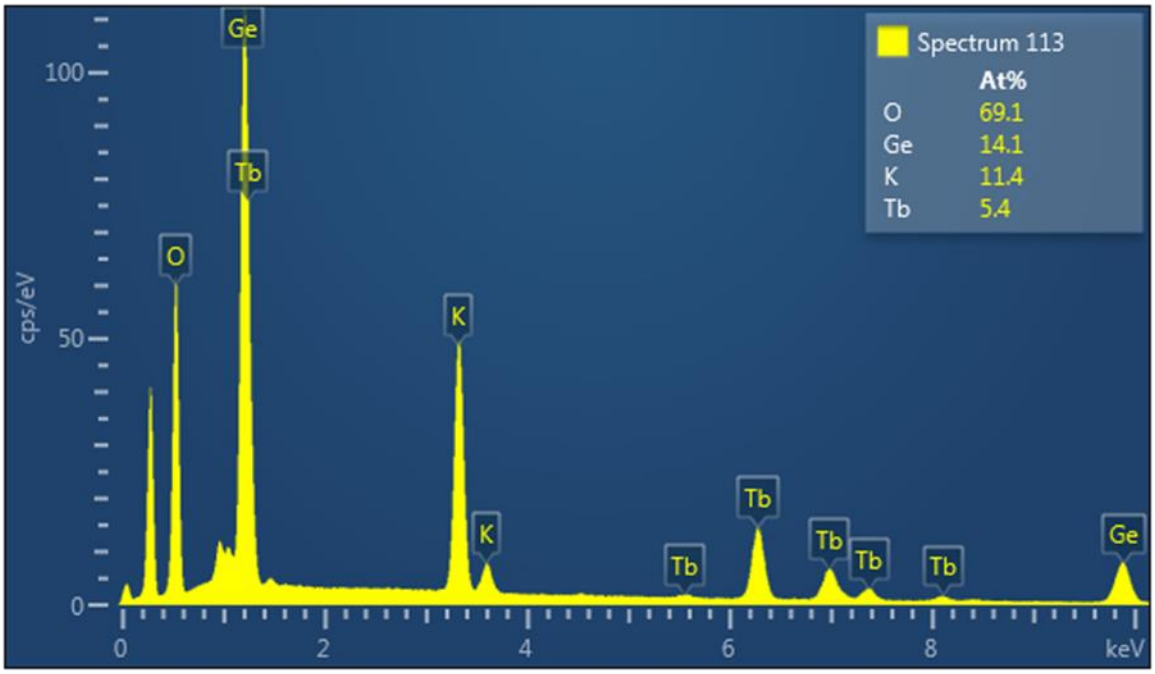


Figure S4. EDX analysis of $K_2TbGe_2O_7$.

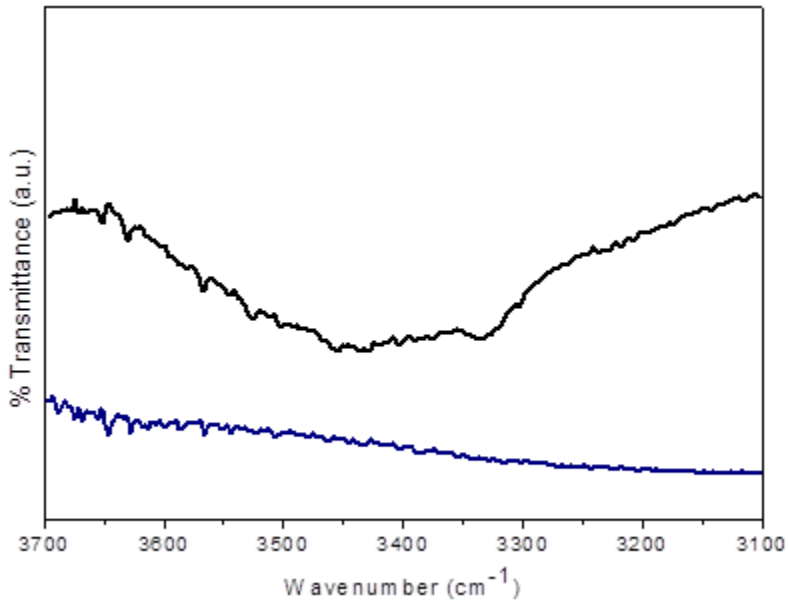


Figure S5. FTIR of the hydroxide stretching regions in $Tb_{13}(GeO_4)_6O_7(OH)$ (black) and $K_2TbGe_2O_7$ (blue) from 3700-3100 $cm^{-1}$.

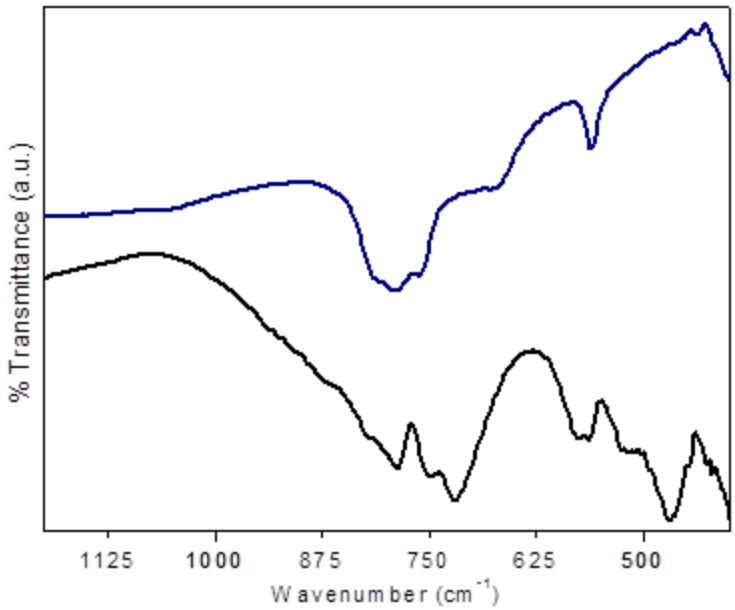


Figure S6. FTIR of germanate regions in $Tb_{13}(GeO_4)_6O_7(OH)$ (black) and $K_2TbGe_2O_7$ (blue) from 1200-400 $cm^{-1}$.

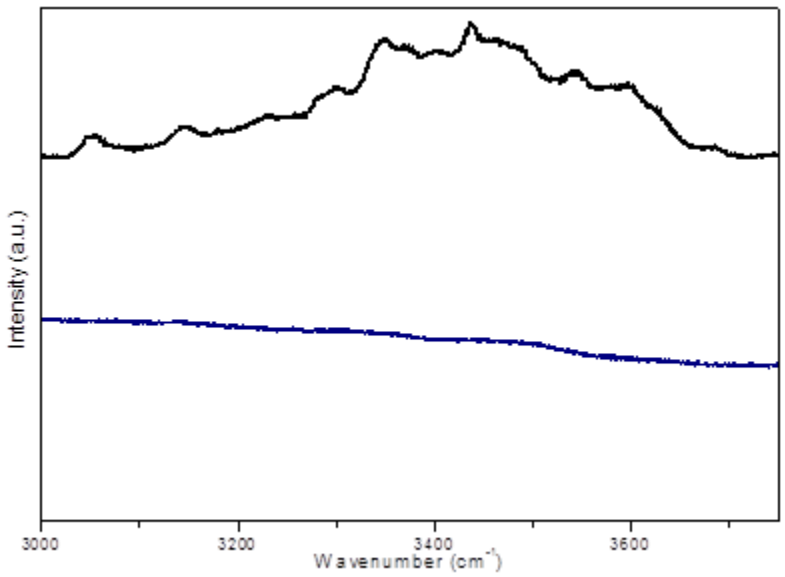


Figure S7. Single crystal Raman scattering of $Tb_{13}(GeO_4)_6O_7(OH)$ (black) and $K_2TbGe_2O_7$ (blue) from 3000-3750 $cm^{-1}$. No presence of hydroxide for $K_2TbGe_2O_7$ was detected. The strongest signal for the $OH^-$ stretching mode for $Tb_{13}(GeO_4)_6O_7(OH)$ occurs at 3437 $cm^{-1}$ in the Raman spectrum, consistent with the broad $OH^-$ feature in the infrared spectrum.

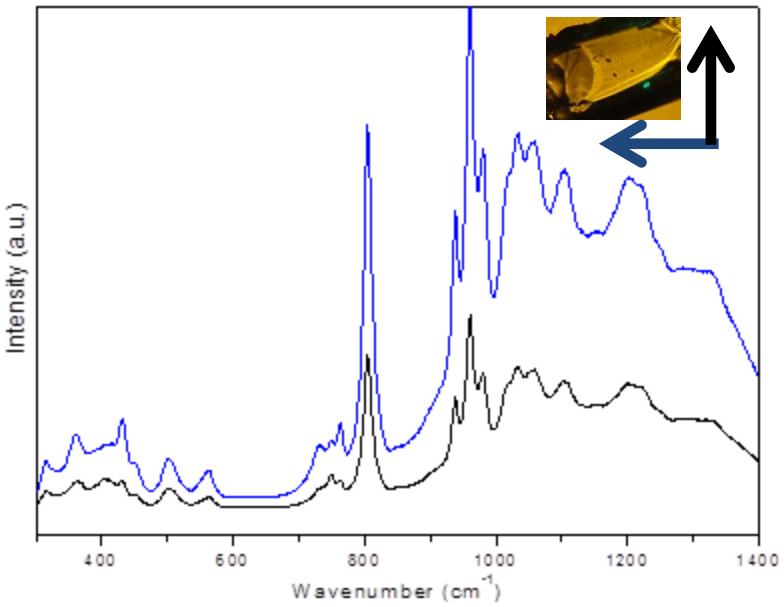


Figure S8. Single crystal Raman scattering of $Tb_{13}(GeO_4)_6O_7(OH)$ from 300-1400 $cm^{-1}$. The intensity ratio of the bands at 749 and 763 $cm^{-1}$ changes as a function of the direction of polarization. Blue indicates polarization left while black indicates polarization up, indicated by direction of arrows.

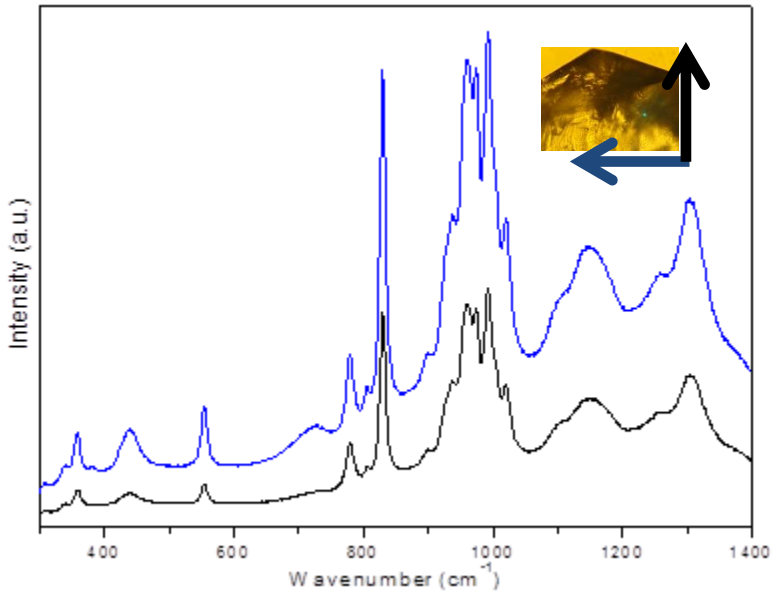


Figure S9. Single crystal Raman scattering of $K_2TbGe_2O_7$ from 300-1400 $cm^{-1}$. No significant changes were observed when the direction of polarization was changed. Blue indicates polarization left while black indicates polarization up, indicated by the direction of the arrows.

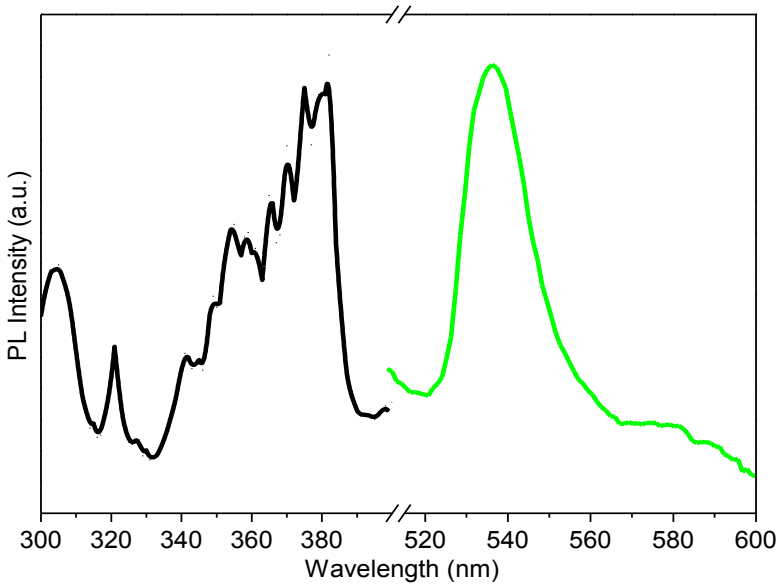


Figure S10. Photoluminescence excitation (black, emission monitored at 535 nm) and emission (green, excited at 380 nm) of $Tb_{13}(GeO_4)_6O_7(OH)$.

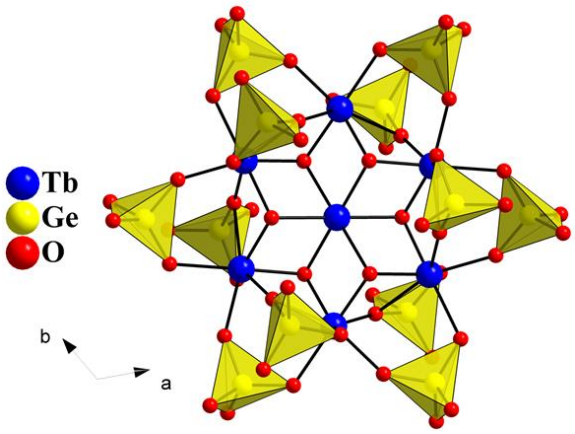


Figure S11. Tb(2)/Tb(3) cluster decorated with isolated $GeO_4$ units viewed along [001] direction.